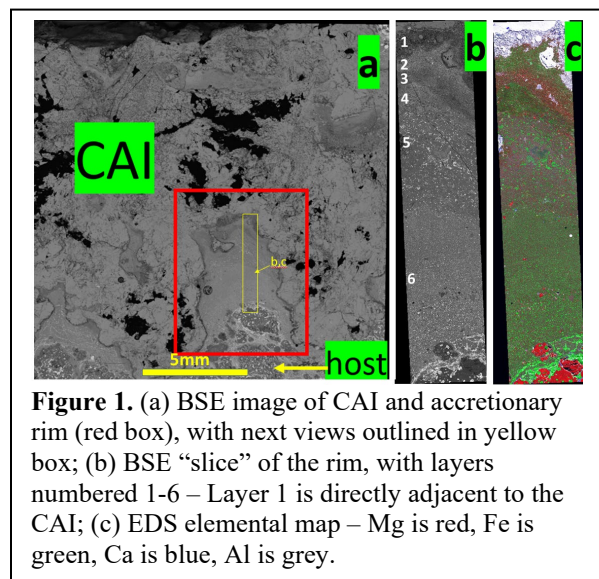


**A MULTILAYERED ACCRETIONARY RIM ON A CAI IN THE NWA 10758 CV3 CHONDRITE.** M. Zolensky<sup>1</sup>, J. Han<sup>2</sup>, L. Le<sup>3</sup>, P. Buchanan<sup>4</sup>, O. Unsalan<sup>5</sup>, C. Altunayar-Unsalan<sup>5,6</sup>; <sup>1</sup>ARES, NASA Johnson Space Center, Houston, TX 77058 USA (michael.e.zolensky@nasa.gov); <sup>2</sup>University of Houston, Houston, TX 77204 USA; <sup>3</sup>Jacobs Technology, Houston, TX 77058 USA; <sup>4</sup>Dept. Geology, Kilgore College, Kilgore, TX 75662 USA; <sup>5</sup>Dept. Physics, Ege University, Izmir, Turkey, <sup>6</sup>Cent. Res. Test. Anal. Lab. Res. App. Cen., Ege University, Izmir, Turkey.

**Introduction:** Northwest Africa (NWA) 10758 is a Bali type oxidized CV3 chondrite, and section JSC1 contains a large (~2.4×1.4 cm), melilite-rich, type A Ca-Al rich inclusion (CAI), briefly introduced before [1,2]. The exceptional feature of this CAI is a thick (locally >5 mm) fine- to coarse-grained, accretionary rim exhibiting at least 6 distinct layers (Fig. 1). This rim may have formed during passage of the still hot CAI through diverse “clouds” of dust, and thus warrants detailed characterization.

**Techniques:** We performed electron beam analyses of the rim, including SEM/EDS (JEOL JSM-7600 FEG-SEM with an Oxford Ultimex EDS) and EPMA (JEOL JXA-8530F FEG-EPMA) on a polished mount, and HRTEM/EDS (JEOL 2500SE STEM with a JEOL SDD EDX) on two FIBs.



**Mineralogy:** The accretionary rim is dominated by olivine Fo40-95, frequently zoned. This range is exceeded by the range for the host Fo19-94. Our element mapping indicates that the olivine compositions are not significantly different between layers. The layers differ in abundance of iron oxides and olivine grain size. Olivine morphologies range from anhedral to euhedral platy crystals. TEM imaging of a FIB slice from the rim layer 4 shows that the olivine crystals are commonly

elongated along the crystallographic C axis. Pyroxenes in the matrix of the rim layer 4 include orthoenstatite and clinoenstatite, frequently intergrown or disordered. Enstatite whisker crystals are present. The accretionary rims have high porosity, although much of the space between olivine crystals is filled with serpentine, identified by lattice fringes of common ~1 nm and ~1.4 nm layers, with rare ~0.7 nm layers, which ranges from poorly crystalline spongy forms to well-crystalline laths (Fig. 2). In some places TEM imaging reveals serpentine forming from breakdown of the olivine. In places the serpentine laths appear to have been deformed where adjacent olivine grains have been pressed against them (Fig. 2c). It is not clear whether this deformation occurred before, during, or after accretion of the rim layer.

Submicron, vesicular objects are locally observed. TEM imaging reveals that these are olivine grains (Fa ~50) containing abundant roughly rectangular pores, which are aligned in their longest dimensions and elongated parallel to the a-axis of the host olivine grains (Fig. 3). These might be the result of dehydration and recrystallization of phyllosilicate laths [3]. Magnetite, with lesser chromite is common within the rim layers, probably a consequence of the post accretionary oxidation that is characteristic of Bali-type CV3 chondrites. Ca phosphates and Fe sulfides are a minor component. Terrestrial weathering is locally significant; thin veinlets of iron oxyhydroxides are present. Fe-Ni sulfides and metal, in particular, have been locally weathered. The observed serpentine is probably not a consequence of terrestrial weathering.

As with other accretionary rims on CAIs, this one contains tiny separate CAIs. We investigated one inclusion (5 μm across) in rim layer 4 (Fig. 4a,b) which consists of melilite and perovskite rimmed by diopside. A larger (~50 μm in size), spherical CAI in rim layer 6 (Fig. 4c,d) consists of melilite containing crystals of perovskite and corundum. These CAIs are in the size range of those found in comet Wild 2 [4].

**Conclusions:** The CAI rim has experienced a significant degree of aqueous alteration. However, the wide compositional range of olivine, preserved olivine zoning, presence of disordered pyroxene and enstatite whisker crystals, and high sample porosity indicate that post-accretionary chemical and physical processing of

the accretionary rim has not been sufficiently severe to completely erase the pre-accretionary mineralogy. Except for the aqueous alteration, these features are similar to those reported for comet Wild 2 and anhydrous chondritic IDPs [4,5]. It may be possible to determine detailed mineralogy of the diverse dust “clouds” that this CAI traversed in the nebula, as each successive layer is characterized.

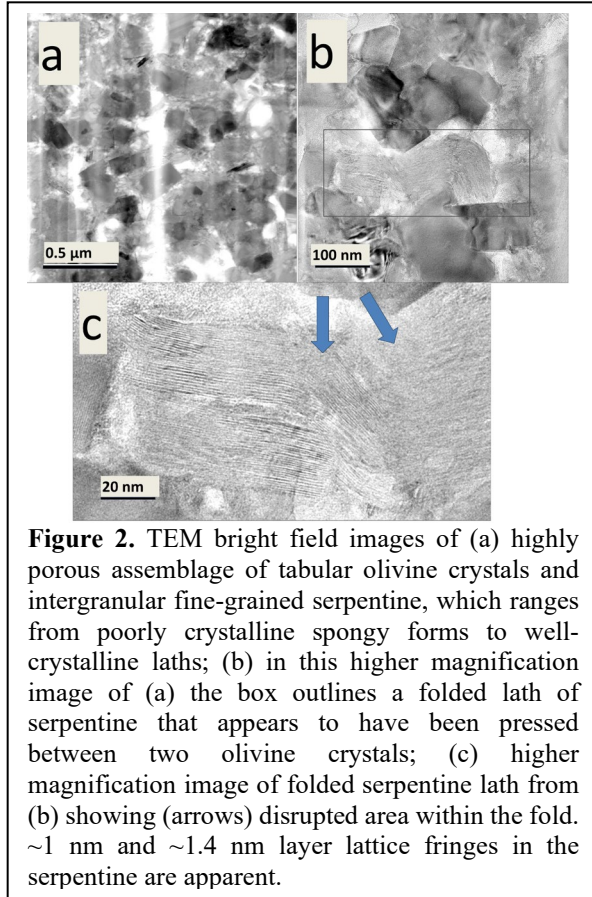


**Figure 2.** TEM bright field images of (a) highly porous assemblage of tabular olivine crystals and intergranular fine-grained serpentine, which ranges from poorly crystalline spongy forms to well-crystalline laths; (b) in this higher magnification image of (a) the box outlines a folded lath of serpentine that appears to have been pressed between two olivine crystals; (c) higher magnification image of folded serpentine lath from (b) showing (arrows) disrupted area within the fold. ~1 nm and ~1.4 nm layer lattice fringes in the serpentine are apparent.

**Acknowledgments:** This work was in part supported by NASA grant 80NSSC21K1558 (JH) and NASA ISFM funding to the JSC Coordinated Analysis Work Package (MZ). OU is supported by Turkish Fulbright Commission under Fulbright Visiting Scholar in 2022-2023 academic year (Grant Number: FY-2022-TR-SS-10).

**References:** [1] Ross et al. (2017) 80th Annual Meeting of the Meteoritical Society, 6378.pdf; [2] Zolensky et al. (2023) *Meteoritical Society Conference Abstracts*; [3] Tonui et al., 2014, *GCA* **126**, 284–306; [4] Zolensky et al., *Science* **314**, 1735-1740; [5] Engrand et al., in *Comets III*, Uni. Ariz Press, in press.

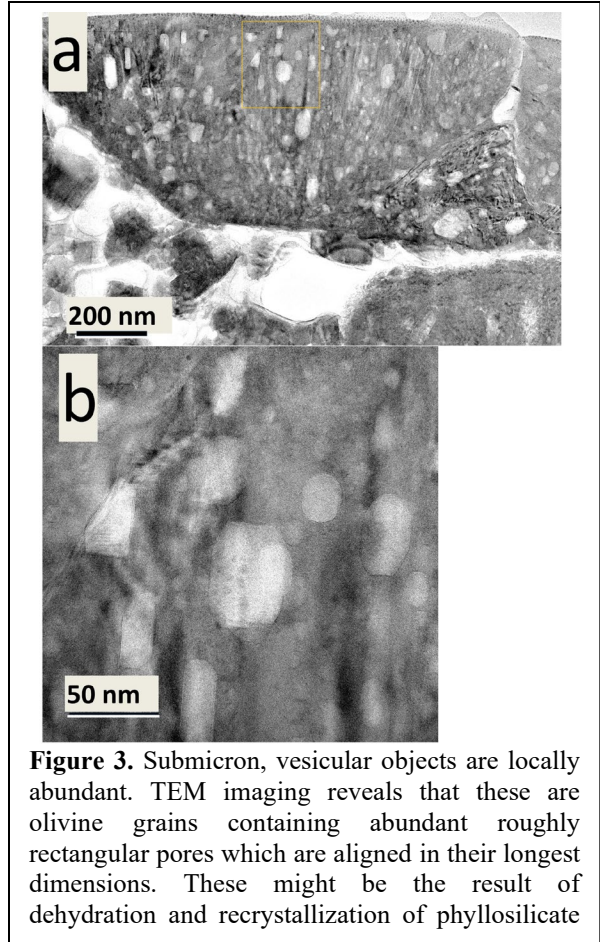


**Figure 3.** Submicron, vesicular objects are locally abundant. TEM imaging reveals that these are olivine grains containing abundant roughly rectangular pores which are aligned in their longest dimensions. These might be the result of dehydration and recrystallization of phyllosilicate

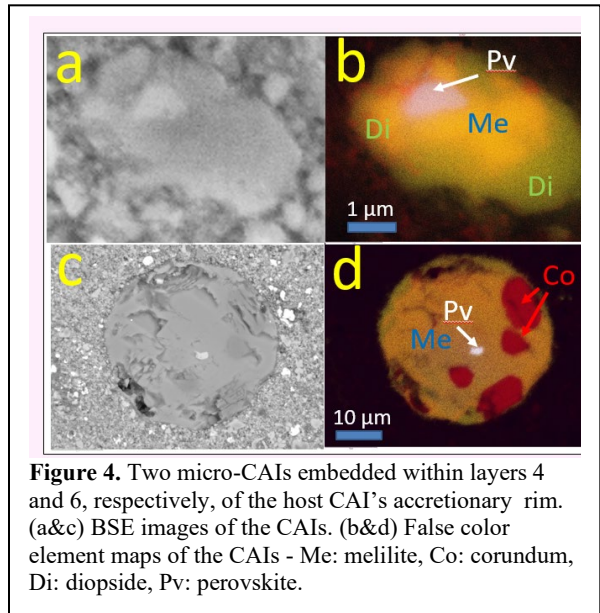


**Figure 4.** Two micro-CAIs embedded within layers 4 and 6, respectively, of the host CAI's accretionary rim. (a&c) BSE images of the CAIs. (b&d) False color element maps of the CAIs - Me: melilite, Co: corundum, Di: diopside, Pv: perovskite.